Research Square

Preprints are preliminary reports that have not undergone peer review.
They should not be considered conclusive, used to inform clinical practice,
or referenced by the media as validated information.

Process-oriented surface modification strategies to optimize interface-only bonding performance of 3D-printed dental polymers

Pyi Phyo Win
Taipei Medical University
Daniel De-Shing Chen
Taipei Medical University
Szu-Yu Lai
Taipei Medical University
Wen-Chieh Hsu
Chung Shan Medical University
Yuichi Mine
Hiroshima University
Tzu-Yu Peng
typeng@tmu.edu.tw

Taipei Medical University

Research Article

Keywords: 3D-printed resin, interface-only bonding, airborne-particle abrasion, resin-matrix penetrating primer, non-thermal handheld plasma

Posted Date: March 30th, 2026

DOI: https://doi.org/10.21203/rs.3.rs-9190061/v1

License: This work is licensed under a Creative Commons Attribution 4.0 International License.
Read Full License

Additional Declarations: No competing interests reported.

Abstract

Current bonding strategies for fixed lingual retainers fabricated with 3D-printed resin (3DR) commonly rely on resin encapsulation or oversized retention pads to compensate for adhesive limitations. While these approaches may enhance bond strength, they compromise the key advantages of additive manufacturing, including streamlined computer-aided design, improved hygiene, and a low-profile structure. To address these limitations, this study proposes an interface-only bonding protocol between additively manufactured resin components that eliminates bulk coverage and pads, placing full reliance on the engineered adhesive interface within the same 3D-printed polymer system. The effectiveness of process-oriented, targeted surface modification strategies, non-thermal handheld plasma (NTHP) and resin matrix-penetrating primer (RMPP), was compared with conventional airborne-particle abrasion (APA) and universal adhesive (UA). Surface characteristics were analyzed using contact profilometry for roughness, water contact angle measurements for wettability, and attenuated total reflectance Fourier-transform infrared spectroscopy (ATR-FTIR) for surface chemical composition of the additively manufactured polymer. Interfacial stability was assessed through shear bond strength (SBS) testing and failure mode analysis before and after 10,000 thermal cycles. The results demonstrate that APA significantly increases surface roughness, while NTHP improves wettability without inducing detectable topographical changes. ATR-FTIR analysis confirmed the presence of distinict urethane dimethacrylate and 10- methacryloyloxydecyl dihydrogen phosphate functional groups in the RMPP and UA groups, respectively, indicating different interfacial chemistries at the 3D-printed polymer–polymer bonding interface. Although pre-aging SBS values were comparable across all groups, the APA–RMPP combination achieved the highest bond stability after aging. In contrast, UA-treated groups exhibited the lowest post-aging values, likely due to increased hydrolytic degradation. These finding suggest that the synergistic effect of micromechanical retention from APA and chemical penetration from RMPP enhances the durability of interface-only bonding between 3D-printed dental polymers of the same material, offering a process-driven, minimalist surface engineering strategy for reliable integration of additively manufactured orthodontic components into modern digital workflows.

1. Introduction

The advent of computer-aided design and computer-aided manufacturing (CAD/CAM) has ushered in a new era of precision and customization in dentistry [1, 2]. Within this digital workflow, additive manufacturing or three-dimensional (3D) printing offers distinct advantages, such as reduced material waste and unique capacity to fabricate complex geometries, over traditional subtractive milling [3]. Recently, 3D-printed resins (3DRs), which were initially developed for permanent crowns, have emerged as a promising alternative material for broader clinical applications. Their proven long-term intraoral stability and favorable mechanical properties make them suitable for the fabrication of fixed lingual retainers (FLRs) [4, 5].

Maintaining orthodontic treatment outcomes remains a persistent challenge as posttreatment relapse threatens to undermine significant investments in time and effort made by both clinicians and patients

[6]. FLRs are frequently indispensable in mitigating this risk, particularly when long-term patient compliance is a concern [7]. For decades, multistranded stainless steel wires have served as the clinical gold standard for fixed retention [8]. However, they possess inherent limitations: manual fabrication is a technique-sensitive process that struggles to achieve a perfectly passive fit, and frequently leads to unwanted tooth movement [9, 10]. Furthermore, the color of these wires can be unesthetic, and their metallic composition can trigger adverse reactions in patients with nickel hypersensitivity, to thereby generate substantial artifacts that compromise the diagnostic quality of magnetic resonance imaging [11, 12].

Despite the potential of 3DRs to resolve these issues, current research frequently replicates traditional “encapsulation” methods and bury the appliance within bulk resin composite or utilize oversized retention pads to compensate for adhesive limitations [13–16]. Although these features increase the bond strength, they negate the clinical benefits of 3D printing, which is a streamlined, hygienic, and low-profile appliance. This study, therefore, evaluates an “interface-only” bonding protocol that eliminates bulk coverage and oversized pads while placing the entire burden of durability on the adhesive interface (Fig. 1).

The translation of 3DRs to this minimalist design introduces a critical challenge: achieving a durable bond to a highly cross-linked polymer network [17, 18]. Conventional surface-modification strategies include airborne-particle abrasion (APA) and universal adhesives (UAs) containing 10-methacryloyloxydecyl dihydrogen phosphate (10-MDP) [19–23]. However, these methods exhibit several limitations. APA is limited by its high operator dependency, as variations in application parameters may compromise the surface consistency and increase the risk of structural defects, especially with the treatment of small and delicate appliances, such as FLRs [24], whereas the chemical bonding efficacy of 10-MDP seems limited to densely cross-linked polymers without prior mechanical roughening [18].

Therefore, several alternative strategies have been developed. Nonthermal handheld plasma (NTHP) offers a minimally invasive approach that increases surface energy and wettability without inducing microstructural damage [25–27]. Resin matrix-penetrating primers (RMPPs) represent a specialized chemical strategy. Originally formulated to condition high-strength, highly cross-linked CAD/CAM composite blocks, these primers contain solvents and functional monomers designed to penetrate and co-polymerize with the resin matrix, and thereby offer a potential pathway for enhanced chemical interaction with structurally analogous 3D-printed materials [28, 29]. Notably, methyl methacrylate (MMA)–containing primers can achieve higher bond strengths than conventional silane agents without APA, and thereby reduce the risk of structural damage [30].

To date, to our knowledge, no study has evaluated the efficacy of NTHP and RMPP for 3DRs in FLR-like geometry using an interface-only protocol or directly compared these methods with conventional APA and UA strategies. In this study, we evaluated the bonding performance of 3DR specimens fabricated in FLR dimensions following NTHP or RMPP surface activation, compared to that achieved with standard protocols.

2. Materials and methods

2.1 Specimen preparation

Specimens were fabricated using the materials detailed in Table 1 based on designs created in SolidWorks (Dassault Systems, Waltham, MA, USA) and exported as STL files. An experienced technician printed the samples using a 3Demax printer (DMG Medical Devices, Hamburg, Germany), following the manufacturer's protocol. Two geometries were produced: disc-shaped specimens (10-mm diameter × 2.5-mm thickness) allocated for surface roughness, water-contact angle (WCA), attenuated total reflectance-Fourier transform infrared (ATR-FTIR) spectroscopy, and SBS testing, and hemi-elliptical specimens (1-mm thickness, 2-mm width, 7-mm length), utilized specifically for SBS analysis. A sample size of 10 specimens per group (n = 10) was used for all quantitative comparisons (surface roughness, WCA, and SBS). After printing, all specimens were polished with a 600-grit abrasive paper and ultrasonically cleaned in distilled water (DW) for 10 min. Surface-treatment procedures were applied to both the disc-shaped and hemi-elliptical specimens. The control group (NT) received no additional surface treatment. For the APA procedure, the specimens were treated with 50-μm Al_2O_3particles at a pressure of 1 bar from 10 mm for 10 s. This was followed by a 5-s rinse with DW and subsequent air-drying. A handheld plasma device (PiezoBrush PZ3, Relyon Plasma GmbH, Regensburg, Germany) was used at 18 W and 50 kHz for 30 s, with a 30-s waiting period before the application of the bonding agent. For UA and RMPP, a single coat of the bonding solution was applied to the entire bonding surface using a microbrush, gently air-dried for approximately 5 s, and then light-cured for 10 s. The specimen classifications and their corresponding abbreviations are listed in Table 2.

Table 1
List of materials used.

Material category	Trade Name (Manufacturer)	Main components and characteristics
3D printed resin (3DR)	Detax freeprint crown (Detax GmbH & Co.KG, Ettlingen, Germany)	Multifunctional methacrylate-based resin (alkoxylated phenol methacrylate derivative, 1,6-hexanediol dimethacrylate, bismethacrylate, photoinitiators, pigments)
Airbone-borne particle abrasion (APA) media	Cobra 50μm (Renfert GmbH, Hilzingen, Germany)	Al_2O_3 particles
Universal adhesive (UA)	3M EPSE Single bond universal (3M ESPE, Seefeld, Germany)	10-MDP, Dimethacrylate resins, HEMA, silane, filler, ethanol, photoinitiators
Resin-matrix penetrating primer (RMPP)	HC primer (SHOFU Inc, Kyoto, Japan)	UDMA, MMA, solvents, initiators
Composite resin	3M Filtek Supreme Flowable restorative (3M ESPE, Seefeld, Germany)	Bis-GMA, TEGDMA, Procrylate, filler, photoinitiators

Details of the compositions were obtained from the manufacturer's safety datasheets. Al_2O_3, aluminum oxide; Bis-GMA, bisphenol a–glycidyl methacrylate; HEMA, 2-hydroxyethyl methacrylate; MDP, methacryloyloxydecyl dihydrogen phosphate; MMA, methyl methacrylate; TEGDMA, triethylene glycol dimethacrylate; UDMA, urethane dimethacrylate.

Table 2 Group classification and corresponding abbreviations for 3D-printed resins subjected to various surface treatments

Abbreviations	Groups
NT	Control group with no surface treatment
AU	Airborne-particle abrasion, followed by universal adhesive application
AP	Airborne-particle abrasion, followed by resin-matrix penetrating primer application
PU	Non-thermal plasma treatment, followed by universal adhesive application
PP	Non-thermal plasma treatment, followed by resin-matrix penetrating primer application

Specifically, for the SBS test, following the respective surface treatments, the bonding surfaces of the hemi-elliptical specimens were coated with composite resin and positioned centrally on the bonding

surfaces of the disc-shaped specimen. Light pressure was applied to ensure proper seating, and excess resin was carefully removed. A light curing unit (Litex 696 Turbo; Dentamerica Inc., City of Industry, CA, USA) was used in regular mode at an intensity of 1200 mW/cm^2 for 40 s. The bonded specimens were stored in distilled water at 37°C for 24 h.

2.2 Evaluation of surface characteristics

Surface roughness (Ra) was measured using a profilometer (Surftest SJ-210, Mitutoyo, Tokyo, Japan) with a cutoff length of 0.8 mm, evaluation length of 6.4 mm, and speed of 0.5 mm/s. Three readings were taken per specimen and the average roughness (Ra) value was calculated. ATR-FTIR analysis (Thermo Scientific Nicolet™ iS™ 10 FTIR Spectrometer, USA) was employed to examine the functional groups resulting from the surface treatment. WCA was assessed using a contact-angle goniometer (Phoenix Mini, Surface Electro Optics Co., Ltd., Suwon, Republic of Korea) with DW. For each specimen, the WCA was measured five times to minimize variability, and the mean value was recorded as the representative WCA.

2.3 Artificial aging and the SBS test

The experimental groups and their corresponding thermocycled counterparts were evaluated. Specimens in the non-aged groups were tested immediately, whereas those in the thermocycled groups underwent 10,000 thermal cycles between 5°C and 55°C, with a 30-s dwell time in each bath. Subsequently, SBS testing was performed using a universal testing machine (JSV-H1000; Japan Instrumentation System Co., Ltd., Nara, Japan) operating at a crosshead speed of 1 mm/min until failure. For each specimen, SBS was calculated by dividing the maximum load at failure by the bonded surface area.

2.4 Failure-pattern evaluation

After the SBS test, the debonded surfaces of the disc specimens were examined using a dental microscope to determine their failure modes. Representative interfaces were documented using a digital stereomicroscope (DMSZ30-C10; Dagong Medical Equipment Co. Ltd., China) at ×0.7 optical magnification, providing an effective magnification of ×20.

Failure modes were classified as follows:

- Adhesive failure: Debonding occurred at the interface between the disc-shaped and hemi-elliptical specimens, with both structures remaining intact.
- Cohesive failure: A fracture or visible crack propagates within the disc-shaped and hemi-elliptical specimens rather than along the bonding interface.
- Mixed failure: Evidence of both interfacial debonding and structural damage to the hemi-elliptical specimen is present. This included cases in which the hemi-elliptical specimen fractured or exhibited a crack line without complete fracture of the disc-shaped specimen.

2.5 Statistical analysis

Statistical analysis was performed using a statistical software program (SPSS 25.0, IBM Corp., Armonk, NY, USA). Data distribution was assessed using the Shapiro–Wilk test. Depending on normality, both roughness and WCA values were analyzed using the Kruskal–Wallis test to compare differences among the surface-treatment groups. For the SBS data, one-way analysis of variance with Tukey's post hoc test was used to compare the surface treatments within the same aging period. The Mann–Whitney *U* test was used to compare the SBS values between the non-thermocycled and thermocycled counterparts within each surface-treatment group. The significance level was set at = 0.05 for all statistical tests.

3. Results and discussion

3.1 Surface characteristics

ATR-FTIR spectroscopy (Fig. 2) revealed classic methacrylate peaks (CH_3, C = O, and C–O) in both UA- and RMPP-treated groups. Notably, the PP group exhibited a distinct N–H stretching peak at approximately 3350 cm^{-1}, corresponding to urethane dimethacrylate (UDMA). The simultaneous appearance of these C–O–C, C = O, CH_3, and N–H signals in the PP group indicates effective chemical bonding [31, 32]. In contrast, the N–H signal in the AP groups was masked by a broad O–H stretching band near 3372 cm^{-1}, possibly owing to residual water remaining after cleaning and rinsing the APA samples. Notably, the distinct Si–O stretching vibration near 1039 cm^{-1} indicates the exposure of the silica fillers. This is consistent with the effective removal of the superficial organic matrix by APA, and thereby unmasks the underlying silica phase. This observation aligns with the findings that Si–O-related signals in adhesive systems are frequently masked by overlapping organic peaks, but can become detectable when surface treatments reduce such interference [33]. For the UA-treated groups, the characteristic methacrylate peaks and C–O stretching bands at 1160 cm^{-1} (AU) and 1156 cm^{-1} (PU) confirmed the presence of 10-MDP [31]. Moreover, the distinct signal of the AU group at 1039 cm^{-1} was attributed to Si–O stretching from the silica filler or P–O from 10-MDP. In the PU group, 1042 cm^{-1} corresponded more to P–O from 10-MDP because NTHP did not expose the filler particles [33].

Table 3 shows the mean Ra values across experimental groups. The NT group showed no significant differences compared with the NTHP-treated specimens ($P < 0.05$). This result is consistent with the know characteristics of NTHP, which has been shown to maintain the original surface morphology [34]. While vacuum plasma is capable of inducing significant surface alterations [35], our findings confirm that the NTHP provides surface activation without modifying the substrate's physical roughness. In contrast, APA significantly increased surface roughness relative to the NT group ($P > 0.05$). Furthermore, the APA-treated groups (AU and AP) exhibited significantly higher roughness than those treated with NTHP (PU and PP) ($P < 0.05$). Although the roughness was lower following RMPP treatment compared to the corresponding UA applications, these differences were not statistically significant ($P > 0.05$). This trend toward reduced surface roughness in the RMPP groups may be attributed to the synergistic effect of the MMA and UDMA monomers. Low-viscosity MMA facilitates deep penetration into the surface micropores, whereas UDMA acts as a cohesive film-former that levels surface irregularities [36]. This

creates a smoother transition layer compared to the UA groups, where the film thickness of one-step UA is frequently < 10 μm and the air-thinning to evaporate solvents further reduces the volume of the adhesive and thereby prevents it from effectively covering all the surface irregularities [37].

Table 3
Surface roughness and water-contact angle of 3D-printed resin after different surface treatments

Groups	Roughness (μm)	Water-contact angle (degree)
NT	0.88 ± 0.07^{A}	95.27 ± 9.85^{a}
AU	2.73 ± 0.22^{B}	15.43 ± 2.55^{b}
AP	1.84 ± 0.19^{B}	49.16 ± 2.57^{c}
PU	0.91 ± 0.28^{A}	17.28 ± 2.47^{b}
PP	0.58 ± 0.17^{A}	50.35 ± 1.32^{c}

Values are expressed as mean ± standard deviation. Within each column, different superscript letters (uppercase for roughness; lower for water-contact angle) indicate statistically significant differences ($P < 0.05$). No statistical comparisons were performed between the data in different columns.

Table 3 presents the mean WCA values across all experimental groups, with the NT group exhibiting the highest hydrophobicity at 95.27 ± 9.85°. This value is comparable to previously reported data for resin post materials (85.2 ± 2.0°), with minor variations likely stemming from differences in material composition [38]. Following surface treatment, all groups showed a significant increase in wettability compared to the NT group ($P < 0.05$). Notably, the UA-treated groups (AU and PU) demonstrated the highest hydrophilicity, with contact angles decreasing significantly to 15.43 ± 2.55° and 17.28 ± 2.47°, respectively; no significant difference was observed between the AU and PU groups ($P > 0.05$). This enhanced wetting is primarily attributed to the inclusion of 2-hydroxyethyl methacrylate (HEMA), a hydrophilic monomer that reduces surface tension and promotes monomer infiltration into the resin microtopography [21]. In contrast, the RMPP-treated groups (AP and PP) exhibited intermediate wettability, with no significant difference observed between them ($P > 0.05$). This response likely results from the formation of a continuous, resin-rich surface layer with elevated surface energy following the infiltration and polymerization of MMA- and UDMA-containing monomers [39].

Ultimately, while surface roughness was primarily governed by the underlying mechanical pretreatments, the WCA was predominantly driven by the different chemical treatments applied.

3.2 Bonding performance

Figure 3 shows the SBS values of the 3DR specimens after the application of various surface treatments. The distribution of failure patterns for each group and representative failure-mode images are presented in Figs. 4 and 5, respectively.

No significant differences in SBS values were observed among the pre-aging groups, regardless of surface pretreatment. This finding is consistent with previous research on permanent 3DR materials that reported comparable SBS across different surface treatments prior to thermocycling [17]. Variations in SBS values may be attributed to differences in 3D-printed material brands, shear body design, and methodological parameters, such as APA pressure and resin cement. To evaluate the clinical viability of these interface-only 3DR retainers, the observed SBS values were benchmarked against the established range of 5.9–7.8 MPa typically required for orthodontic brackets to withstand masticatory forces [40]. Notably, the SBS of all experimental groups fell within or approached this threshold limit: the NT, AU, AP, PU, and PP groups at 5.82 ± 1.66, 6.91 ± 1.95, 7.24 ± 1.46, 6.91 ± 1.40, and 6.75 ± 1.13 MPa, respectively. The hemi-elliptical shear body design was used in this study based on its favorable flexural strength and suitability for the FLR [5]. These values indicate that even with a streamlined, interface-only design, the 3DR can provide sufficient initial adhesion for clinical applications. Therefore, a hemi-elliptical shape was chosen to provide clinically relevant bonding conditions applicable to all permanent indirect prostheses, including the FLR. APA was performed at 1 bar because higher pressures do not provide additional SBS benefits and may increase the risk of substrate damage [41]. Failure-mode analysis revealed predominantly mixed failures in the NT group (63.64%), whereas surface-treated groups showed a higher incidence of cohesive failures, including AU (81.82%), AP (90.91%), PU (72.73%), and PP (72.73%). This shift indicates that failure was primarily governed by the material strength rather than the interfacial bond integrity. Although the NT group exhibited a substantial proportion of mixed failure (63.64%), the presence of adhesive failure (9.09%) suggested a more interface-dependent bonding behavior with reduced stress transfer into the substrate. Cohesive and mixed failure modes are generally considered more favorable than adhesive failure because the latter is typically associated with a lower bond strength [42, 43]. Moreover, no adhesive failure was observed in the surface-treated groups, which exclusively exhibited cohesive or mixed failures. Specifically, APA produced a high rate of cohesive failure (AU: 81.82% and AP: 90.91%), likely owing to enhanced micromechanical retention from surface roughening, consistent with previous findings [44]. Moreover, the NTHP-treated groups demonstrated high cohesive failure rates accompanied by mixed failures, suggesting a balanced enhancement of surface chemical reactivity and micromechanical features.

The integrity of the bond was significantly compromised by aging, as all groups exhibited a significant reduction in SBS, ranging from 26.93% to 69.75% relative to their non-aged counterparts ($P < 0.01$). Despite the general decline in strength, the AP group maintained a mean SBS of 5.29 ± 1.47 MPa after thermocycling, which is significantly higher than the values seen in NT (3.17 ± 1.10 MPa) and groups utilizing UA (AU: 2.09 ± 1.37 MPa and PU: 2.38 ± 0.35 MPa). The intergroup comparisons showed that NT, AU, PU, and PP were not significantly different from one another, and PP (3.84 ± 0.79 MPa) did not differ from any group. Only the AP group exhibited significantly different SBS values, and this difference was not observed when compared to the PP group. While these aged values are slightly below the immediate, non-aged 5.9–7.8 MPa bracket benchmark, they must be interpreted within the context of modern digital workflows. Owing to digital fabrication, 3D-printed FLRs can be accurately designed and positioned outside the direct occlusion, thereby minimizing the shear stresses encountered during masticatory

function. In such protected clinical environments, the sustained interfacial stability of the AP group suggests that the combination of APA and RMPP provides sufficient durability for a streamlined interface-only design. UA-treated groups exhibited the greatest reduction in SBS after thermocycling, with decreases of 69.75% for AU and 65.56% for PU. Moreover, the predominant failure mode of UA-treated groups shifted from cohesive to mainly adhesive after thermocycling, with AU exhibiting 90.91% adhesive failure and PU reaching 100%, indicating reduced interfacial integrity after aging. This deterioration was likely related to the presence of HEMA, which enhanced wettability but promoted water sorption and hydrolytic degradation over time [21]. These findings were consistent with previous reports on the reduced long-term stability of HEMA-containing adhesives [45]. Notably, the NT group maintained relatively higher SBS values and predominantly mixed failures, despite no significant differences compared to the UA-treated group. This trend is consistent with previous findings showing the limited benefit of UA application to untreated or APA-treated 3DR surfaces [17]. The lack of improvement in the PP group further suggests that NTHP does not alter the surface topography and that RMPP requires mechanical surface modification for effective interactions. This contrast with vacuum plasma treatment which optimizes 3DR adhesion by inducing a “corrosion effect” and creating micropores [34]. After pre-aging, although the PP group exhibited SBS values similar to those of the AP group, the differences were non-significant in the remaining groups. The adhesive failure in the PP group (45.45%) after aging indicated that its bond reliability was not equivalent to that of the AP group (0%). Overall, the AP group demonstrated the most favorable performance and achieved the highest SBS after thermocycling and superior interfacial stability. Its reliability was supported by the failure mode analysis, which revealed 54.55% cohesive and 45.45% mixed failures, without adhesive failures. The sustained bonding performance after thermocycling may be attributed to the synergistic interaction between the mechanical roughening and chemical priming. APA generates surface irregularities for micromechanical retention, whereas the low-molecular-weight MMA monomers in RMPP deeply penetrate these features, capitalizing on 3DR’s high matrix availability [28, 29]. This combination reduces the water permeability and effectively resists hydrolytic degradation, which is typical of thermal aging.

Although the initial SBS values were comparable across all the surface-treatment groups, the APA-treated specimens exhibited a higher frequency of cohesive failure before aging. The occurrence of fractures in the thicker disc-shaped specimen suggests a reduction in the structural integrity of the material. Nevertheless, the AP group maintained the best performance following aging compared to the other treatments, which underscores that the benefits of mechanical interlocking may outweigh the slight compromise in material strength.

This study had some limitations. As an in vitro investigation, it cannot replicate all conditions of the oral environment. These findings are specific to a single brand of 3DR and the resin composite cement. The bonding performance was primarily evaluated through SBS testing after thermocycling, which represents only one mode of mechanical loading and one method of artificial aging. Future research should consider long-term aging models, different mechanical methods, and a broader range of commercially available materials to enhance the clinical translatability.

5. Conclusion

Within the limitations of this in vitro study, the following conclusions were drawn:

1. APA significantly enhanced mechanical bonding by generating deeper micromechanical retention, whereas the portable NTHP treatment did not provide any measurable benefits under the tested conditions.
2. UA induced the highest hydrophilicity owing to its high HEMA content, followed by RMPP, which formed a hydrophilic resin-rich layer. Notably, the lack of a significant difference between APA and NTHP when paired with the same chemical treatment suggests that chemical treatments masked the underlying mechanical pretreatment.
3. An interface-only design is clinically viable when the mechanical reinforcement of traditional encapsulation is replaced by the high-performance surface treatment of APA–RMPP. By using 3D printing to place the retainer out of direct occlusion and ensure a robust chemical-mechanical bond, clinicians can provide a more aesthetic, hygienic, and streamlined appliance without sacrificing durability.

Declarations

Author Contribution

P.P.W. wrote the main manuscript text and performed the formal analysis, data curation, investigation, and software-based methodology. T.-Y.P. was responsible for the conceptualization, resources, and the final review and editing of the manuscript. D.D.-S.C., W.-C.H., and Y.M. provided overall supervision, validation, and visualization of the data. S.-Y.L. assisted with data curation, investigation, and formal analysis. All authors reviewed and approved the final version of the manuscript.

Acknowledgement

The authors would like to thank the National Science and Technology Council of Taiwan for their financial support of this research.

References

1. Alhallak K, Hagi-Pavli E, Nankali A (2023) A review on clinical use of CAD/CAM and 3D printed dentures. Br Dent J. https://doi.org/10.1038/s41415-022-5401-5
2. Holban CC, Tatarciuc M, Vitalariu AM, Vasluianu RI, Antohe M, Diaconu DA, Stamatin O, Dima AM (2025) Three-dimensional printing and CAD/CAM milling in prosthodontics: a scoping review of key metrics towards future perspectives. J Clin Med 14:4837. https://doi.org/10.3390/jcm14144837

3. Jun MK, Kim JW, Ku HM (2025) Three-dimensional printing in dentistry: a scoping review of clinical applications, advantages, and current limitations. Oral 5:24. https://doi.org/10.3390/oral5020024
4. Firlej M, Zaborowicz K, Zaborowicz M, Firlej E, Domagala I, Pieniak D, Igielska-Kalwat J, Dmowski A, Biedziak B (2022) Mechanical properties of 3D printed orthodontic retainers. Int J Environ Res Public Health 19:5775. https://doi.org/10.3390/ijerph19095775
5. Win PP, Lai SY, Chen DS, Sainbayar B, Peng TY, Cheng HC (2025) Evaluation of the physical and mechanical properties of 3D-printed resin for orthodontic fixed lingual retainers: An in vitro study. J Dent Sci 20:1723–1730. https://doi.org/10.1016/j.jds.2025.03.034
6. Littlewood SJ, Dalci O, Dolce C, Holliday LS, Naraghi S (2021) Orthodontic retention: what's on the horizon?. Br Dent J 230:760–764. https://doi.org/10.1038/s41415-021-2937-8
7. Al-Moghrabi D, Johal A, O'Rourke N, Donos N, Pandis N, Gonzales-Marin C, Fleming PS (2018) Effects of fixed vs removable orthodontic retainers on stability and periodontal health: 4-year follow-up of a randomized controlled trial. Am J Orthod Dentofac Orthop 154:167–174. https://doi.org/10.1016/j.ajodo.2018.01.007
8. Zachrisson BU (2015) Multistranded wire bonded retainers: from start to success. Am J Orthod Dentofac Orthop 148:724–727. https://doi.org/10.1016/j.ajodo.2015.07.015
9. Shaughnessy TG, Proffit WR, Samara SA (2016) Inadvertent tooth movement with fixed lingual retainers. Am J Orthod Dentofac Orthop 149:277–286. https://doi.org/10.1016/j.ajodo.2015.10.015
10. Seide M, Kruse T, Graf I, Bourauel C, Lapatki BG, Jäger R, Braumann B (2024) Inadvertent side effects of fixed lingual retainers: an in vitro study. J Orofac Orthop 85:223–232. https://doi.org/10.1007/s00056-022-00432-4
11. Shalish M, Dykstein N, Friedlander-Barenboim S, Ben-David E, Gomori JM, Chaushu S (2015) Influence of common fixed retainers on the diagnostic quality of cranial magnetic resonance images. Am J Orthod Dentofac Orthop 147:604–609. https://doi.org/10.1016/j.ajodo.2014.11.022
12. Roser C, Hilgenfeld T, Sen S, Badrow T, Zingler S, Heiland S, Bendszus M, Lux CJ, Juerchott A (2021) Evaluation of magnetic resonance imaging artifacts caused by fixed orthodontic CAD/CAM retainers-an in vitro study. Clin Oral Investig 25:1423–1431. https://doi.org/10.1007/s00784-020-03450-x
13. Alnuaimy NS, Alhuwaizi AF (2025) Debonding forces and failure modes of customized three-dimensional printed nano-ceramic hybrid resin fixed lingual retainers. J Orthod Sci 14:2. https://doi.org/10.4103/jos.jos_75_24
14. Kadhum AS, Alhuwaizi AF (2021) The efficacy of polyether-ether-ketone wire as a retainer following orthodontic treatment. Clin Exp Dent Res 7:302–312. https://doi.org/10.1002/cre2.377
15. Aboulazm K, von See C, Othman A (2021) Fixed lingual orthodontic retainer with bilateral missing lateral incisors produced in PEEK material using CAD/CAM technology. J Clin Exp Dent 13:e549–e551. https://doi.org/10.4317/jced.58035
16. Alabbadi AA, Abdalla EM, Hanafy SA, Yousry TN (2023) A comparative study of CAD/CAM fabricated polyether ether ketone and fiber-glass reinforcement composites versus metal lingual retainers

under vertical load (an in vitro study). BMC Oral Health 23:583. https://doi.org/10.1186/s12903-023-03268-5

17. Kang YJ, Park Y, Shin Y, Kim JH (2023) Effect of adhesion conditions on the shear bond strength of 3D printing resins after thermocycling used for definitive prosthesis. Polymers (Basel) 15:1390. https://doi.org/10.3390/polym15061390
18. Bourgi R, Etienne O, Holiel AA, Cuevas-Suárez CE, Hardan L, Roman T, Flores-Ledesma A, Qaddomi M, Haikel Y, Kharouf N (2025) Effectiveness of surface treatments on the bond strength to 3D-printed resins: a systematic review and meta-analysis. Prosthesis 7:0056. https://doi.org/10.3390/prosthesis7030056
19. Kömürcüoğlu MB, Sağırkaya E, Tulga A (2017) Influence of different surface treatments on bond strength of novel CAD/CAM restorative materials to resin cement. J Adv Prosthodont 9:439–446. https://doi.org/10.4047/jap.2017.9.6.439
20. Graf T, Erdelt KJ, Guth JF, Edelhoff D, Schubert O, Schweiger J (2022) Influence of pre-treatment and artificial aging on the retention of 3D-printed permanent composite crowns. Biomedicines 10:2186. https://doi.org/10.3390/biomedicines10092186
21. Arandi NZ (2023) The classification and selection of adhesive agents; an overview for the general dentist. Clin Cosmet Investig Dent 15:165–180. https://doi.org/10.2147/ccide.s425024
22. Ersöz B, Ezmek B, Karaoğlanoğlu S, Çal İK (2024) Effect of surface treatment applied to 3D printed permanent resin on shear bond strength. J Clin Exp Dent 16:e1059–1066. https://doi.org/10.4317/jced.61884
23. Sutuven EO, Yildirim NC (2025) Bond strength of self-adhesive resin cement to definitive resin crown materials manufactured by additive and subtractive methods. Dent Mater J 44:41–51. https://doi.org/10.4012/dmj.2024-111
24. Gama LT, Duque TM, Özcan M, Philippi AG, Mezzomo LA, Gonçalves TM (2020) Adhesion to high-performance polymers applied in dentistry: a systematic review. Dent Mater 36:e93–e108. https://doi.org/10.1016/j.dental.2020.01.002
25. Dede DÖ, Ercan UK, Küçükekenci AS, Kahveci Ç, Özdemir GD, Bağış B (2021) Influence of non-thermal plasma systems and two favorable surface treatments on the shear bond strength of PAEKs to composite resin. J Adhes Sci Technol 36:748–761. https://doi.org/10.1080/01694243.2021.1936784
26. Tseng CF, Lee IT, Wu SH, Chen HM, Mine Y, Peng TY, Kok SH (2024) Effects of handheld nonthermal plasma on the biological responses, mineralization, and inflammatory reactions of polyaryletherketone implant materials. J Dent Sci 19:2018–2026. https://doi.org/10.1016/j.jds.2024.06.014
27. Zhong G, Xu S, Yu C, Atashbahar M, Liu Q (2026) Effect of non-thermal atmospheric plasma treatment on bonding performance of customized ceramic post-and-cores. J Esthet Restor Dent 38:143–155. https://doi.org/10.1111/jerd.70031

28. Morikawa Y, Ouchi S, Yoshikawa K, Yamamoto K (2019) Effect of an experimental primer solution on bonding to resin blocks. Jpn J Conserv Dent 62:8–16. https://doi.org/10.11471/shikahozon.62.8
29. Hagino R, Mine A, Matsumoto M, Yumitate M, Ban S, Yamanaka A, Ishida M, Miura J, Van Meerbeek B, Yatani H (2021) Combination of a silane coupling agent and resin primer reinforces bonding effectiveness to a CAD/CAM indirect resin composite block. Dent Mater J 40:1445–1452. https://doi.org/10.4012/dmj.2021-083
30. Asakura M, Aimu K, Hayashi T, Matsubara M, Mieki A, Ban S, Kawai T (2023) Bonding characteristics of silane coupling agent and MMA-containing primer to various composite CAD/CAM blocks. Polymers (Basel) 15:3396. https://doi.org/10.3390/polym15163396
31. Almusa A, Delgado AH, Ashley P, Young AM (2021) Determination of dental adhesive composition throughout solvent drying and polymerization using ATR-FTIR spectroscopy. Polymers (Basel) 13:2238. https://doi.org/10.3390/polym13223886
32. Huang HY, Feng SW, Chiang KY, Li YC, Peng TY, Nikawa H (2024) Effects of various functional monomers' reaction on the surface characteristics and bonding performance of polyetheretherketone. J Prosthodont Res 68:319–325. https://doi.org/10.2186/jpr.jpr_d_23_00063
33. Yoshihara K, Nagaoka N, Sonoda A, Maruo Y, Makita Y, Okihara T, Irie M, Yoshida Y, Van Meerbeek B (2016) Effectiveness and stability of silane coupling agent incorporated in 'universal' adhesives. Dent Mater 32:1218–1225. https://doi.org/10.1016/j.dental.2016.07.002
34. Arrieta JA, Vargas I, Solis Y (2015) Atmospheric-Pressure Non-thermal Plasma-JET effects on PS and PE surfaces. J Phys Conf Ser 591:012050. https://doi.org/10.1088/1742-6596/591/1/012050
35. Lee M, Kang YJ, Park Y, Jeon HJ, Kim JH (2025) Effect of vacuum plasma treatment on the shear bond strength of 3D-printed resin and self-adhesive resin cement. Dent Mater J 44:211–219. https://doi.org/10.4012/dmj.2024-128
36. Alabdali ZN, Reiter MP, Lynch-Branzoi JK, Mann AB (2020) Compositional effects on mechanical properties and viscosity in UDMA-MMA blends. J Adhes Sci Technol 35:610–625. https://doi.org/10.1080/01694243.2020.1816779
37. Kharouf N, Ashi T, Eid A, Maguina L, Zghal J, Sekayan N, Bourgi R, Hardan L, Sauro S, Haikel Y, Mancino D (2021) Does adhesive layer thickness and tag length influence short/long-term bond strength of universal adhesive systems? an in-vitro study. Appl Sci 11:2635. https://doi.org/10.3390/app11062635
38. Küden C, Batmaz SG, Karakas SN (2024) Enhancing bond strength of 3D-printed resin posts using various surface pretreatments: an in vitro study. Int J Prosthodont 37:253–263. https://doi.org/10.11607/ijp.8914
39. Prabriputaloong S, Krajangta N, Klaisiri A (2025) The effect of different chemical surface treatments on the bond strength of resin-matrix ceramic repaired with resin composite. Eur J Dent 19:165–172. https://doi.org/10.1055/s-0044-1785531
40. Reynolds IR (1976) A review of direct orthodontic bonding. Br J Orthod 2:171–178. https://doi.org/10.1080/0301228x.1975.11743666

41. Dederichs M, Badr Z, Viebranz S, Nietzsche S, Schulze-Spate U, Schmelzer AS, Lehmann T, Guentsch A (2025) Effect of surface conditioning on the adhesive bond strength of 3D-printed resins used in permanent fixed dental prostheses. J Dent 155:105621. https://doi.org/10.1016/j.jdent.2025.105621
42. Secilmis A, Ustun O, Buyukhatipoglu IK (2016) Evaluation of the shear bond strength of two resin cements on different CAD/CAM materials. J Adhes Sci Technol 30:983–993. https://doi.org/10.1080/01694243.2015.1134866
43. Alp G, Subaş MG, Johnston WM, Yilmaz B (2018) Effect of different resin cements and surface treatments on the shear bond strength of ceramic-glass polymer materials. J Prosthet Dent 120:454–461. https://doi.org/10.1016/j.prosdent.2017.12.016
44. Kim SY, Shin Y, Kim IH, Song JS (2023) In vitro study on the bond strength between 3D-printed resin and resin cement for pediatric crown restoration. J Korean Acad Pediatr Dent 50:104–112. https://doi.org/10.5933/jkapd.2023.50.1.104
45. Silva TSP, Castro RF, Magno MB, Maia LC, Silva ESMHJ (2018) Do HEMA-free adhesive systems have better clinical performance than HEMA-containing systems in noncarious cervical lesions? a systematic review and meta-analysis. J Dent 74:1–14. https://doi.org/10.1016/j.jdent.2018.04.005

Figures

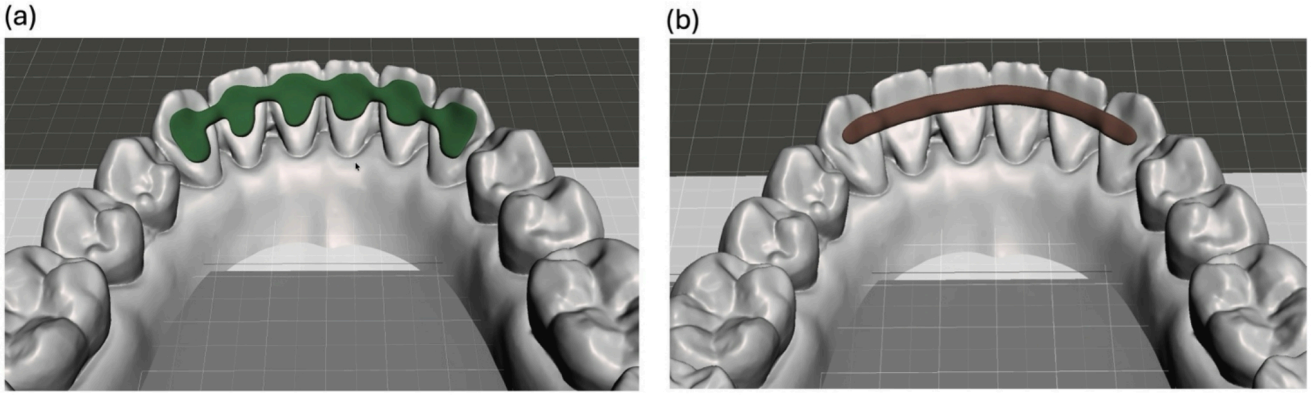


Figure 1

Virtual models of 3D-printed fixed lingual retainers on a mandibular arch: a design utilizing retention pad for enhanced surface contact (green); b minimalist, interface-only design (brown)

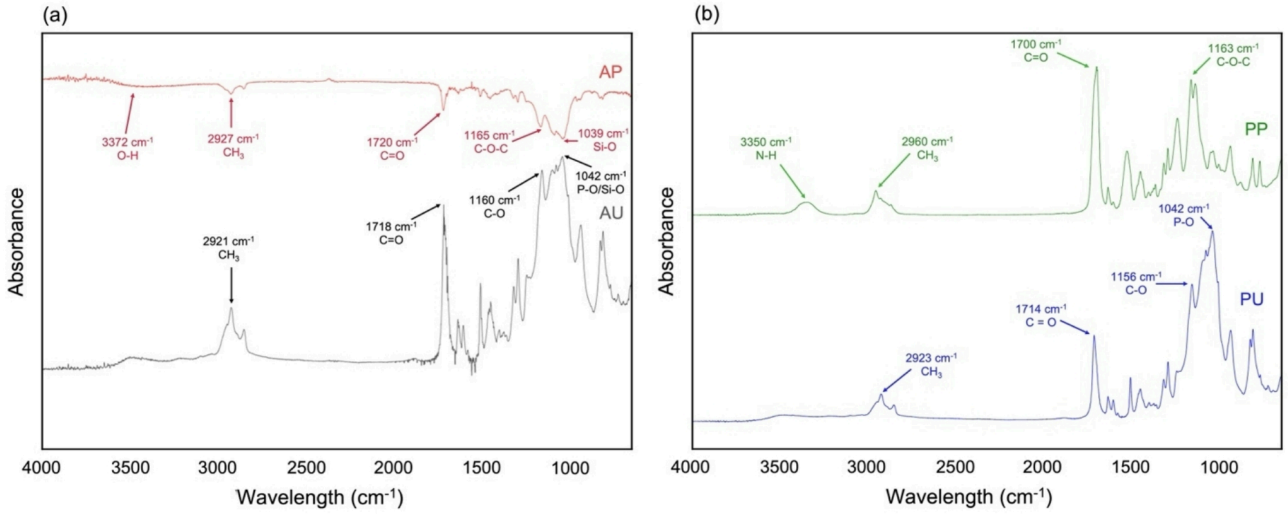


Figure 2

ATR-FTIR analysis of 3D-printed resin specimens following different surface treatments: **a** AP–airborne-particle abrasion (APA) followed by resin-matrix penetrating primer (RMPP) application and AU–APA followed by universal adhesive (UA) application; **b** PP–non-thermal handheld plasma (NTHP) treatment followed by RMPP application and PU–NTHP treatment followed by UA application

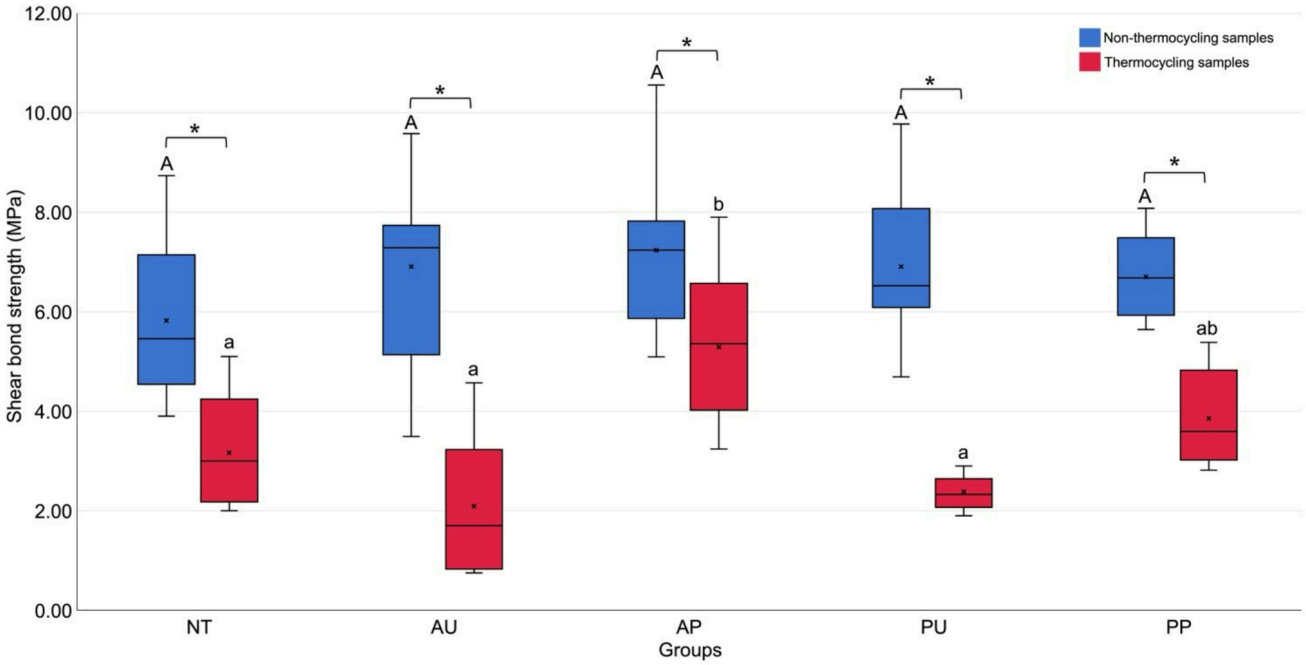


Figure 3

Shear bond strength of 3D-printed resin specimens subjected to different surface treatments before and after thermocycling

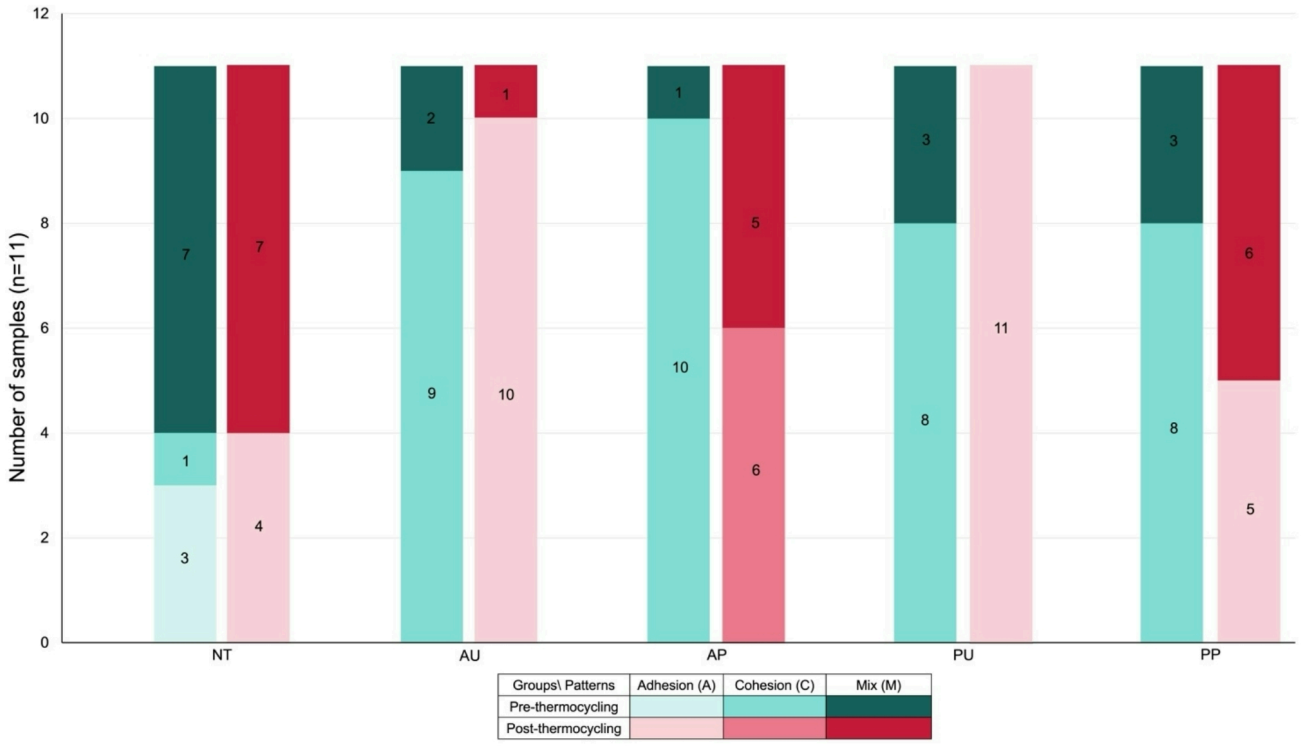


Figure 4

Distribution of fracture patterns of 3D-printed resin specimens across different surface treatments before and after thermocycling

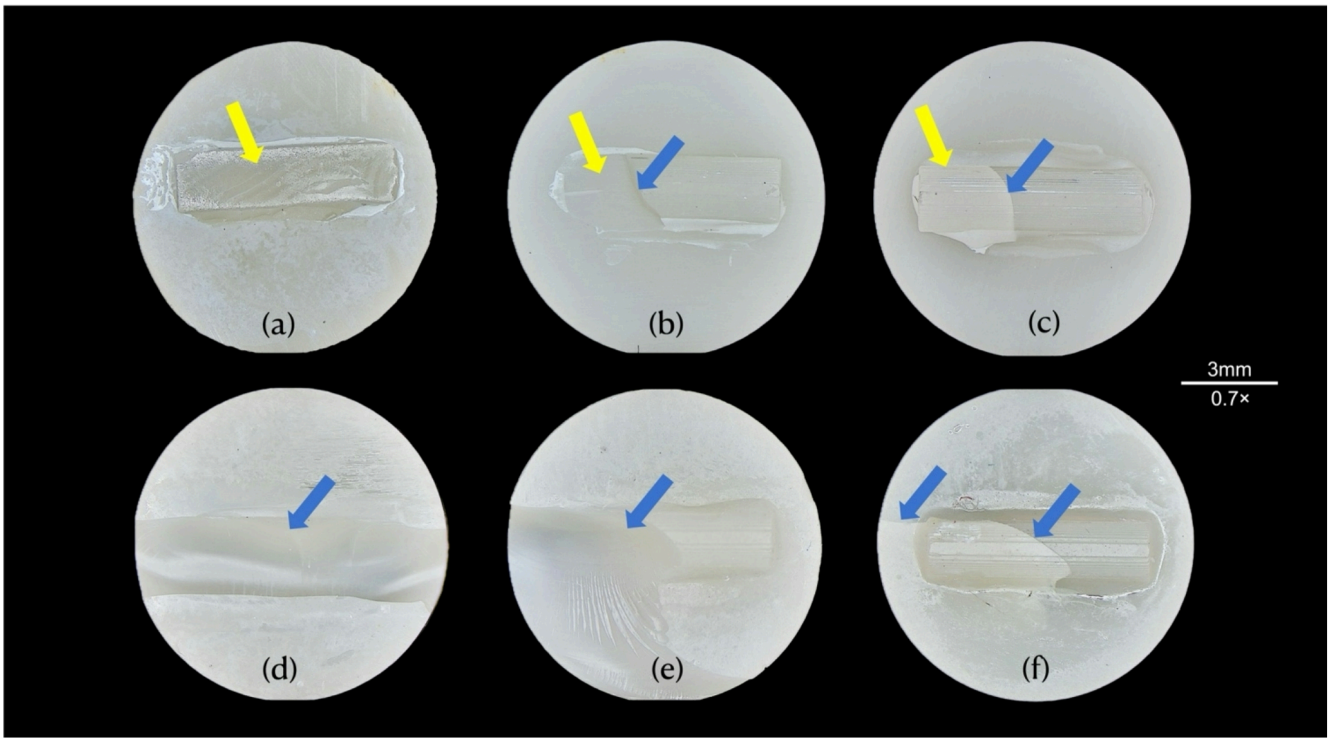


Figure 5

Microscopic illustration of fracture patterns, captured at ×0.7 optical magnification (effective magnification of ×20), reveals: **a** adhesive failure; **b, c** mixed failure; and **d, e, f**cohesive failure with yellow arrows indicate failure at the bonding interface and blue arrows indicate failure within the 3D-printed resin specimens